IMMUNOLOGY

De novo phosphorylation and conformational opening of the tyrosine kinase Lck act in concert to initiate T cell receptor signaling

Lars Philipsen,[1]* Amarendra V. Reddycherla,[1]* Roland Hartig,[1] Janine Gumz,[1] Matthias Kästle,[1] Andreas Kritikos,[1] Mateusz P. Poltorak,[1] Yury Prokazov,[2] Evgeny Turbin,[2] André Weber,[2] Werner Zuschratter,[2] Burkhart Schraven,[1,3]*† Luca Simeoni,[1]*† Andreas J. Müller[1,4]*†

The enzymatic activity of the Src family tyrosine kinase p56^{Lck} (Lck) is tightly controlled by differential phosphorylation of two tyrosine residues, Tyr^{394} and Tyr^{505}. Phosphorylation of Tyr^{394} and the conformational opening of Lck are believed to activate the kinase, whereas Tyr^{505} phosphorylation is thought to generate a closed, inactive conformation of Lck. We investigated whether the conformation of Lck and its phosphorylation state act in concert to regulate the initiation of T cell receptor (TCR) signaling. With a sensitive biosensor, we used fluorescence lifetime imaging microscopy (FLIM) to investigate the conformations of wild-type Lck and its phosphorylation-deficient mutants Y394F and Y505F and the double mutant Y394F/Y505F in unstimulated T cells and after TCR stimulation. With this approach, we separated the conformational changes of Lck from the phosphorylation state of its regulatory tyrosines. We showed that the conformational opening of Lck alone was insufficient to initiate signaling events in T cells. Rather, Lck additionally required phosphorylation of Tyr^{394} to induce T cell activation. Consistent with the FLIM measurements, an optimized immunofluorescence microscopy protocol revealed that the TCR-stimulated phosphorylation of Lck at Tyr^{394} occurred preferentially at the plasma membrane of Jurkat cells and primary human T cells. Our study supports the hypothesis that T cell activation through the TCR complex is accompanied by the de novo activation of Lck and that phosphorylation of Tyr^{394} plays a role in Lck function that goes beyond inducing an open conformation of the kinase.

INTRODUCTION

The protein tyrosine kinase p56^{Lck} (hereafter termed Lck), a member of the Src family of protein tyrosine kinases, plays a central role in the development, homeostasis, and activation of T cells. Mice deficient in Lck lack peripheral T cells because of a block at the double negative 3 (DN3) stage of thymocyte development (*1*). Moreover, loss of *lck* in peripheral T lymphocytes results in impaired homeostatic T cell proliferation (*2*). Finally, deletion of *lck* in Jurkat cells (a human CD4$^+$ T cell leukemia line) completely blocks early T cell receptor (TCR)–mediated signals, such as the induction of Ca^{2+} flux or the activation of extracellular signal–regulated kinase (ERK) (*3*).

Lck initiates T cell activation by phosphorylating the so-called immunoreceptor tyrosine-based activation motifs (ITAMs), 10 of which are present in the cytoplasmic domains of the TCR-associated CD3 and ζ chains (*4*). Phosphorylation of ITAMs by Lck enables activated T cells to recruit the Syk family kinase ζ-associated phosphoprotein of 70 kD (ZAP70) to the activated TCR-CD3-ζ complex. In turn, ZAP70 is phosphorylated and activated by Lck, thereby stimulating the tyrosine phosphorylation of the transmembrane adaptor protein linker for activation of T cells (LAT), a molecular hub that connects the activated TCR to many downstream signaling pathways. However, despite two decades of intense research, the mechanism by which Lck causes ITAM phosphorylation is still unclear. The so-called "standby" model is based on the assumption that the enzymatic activity of Lck does not change after the TCR is engaged by antigen (*5*). Rather, this model proposes that ITAM phosphorylation is initiated by the TCR-induced redistribution of constitutively activated Lck within the cell or that TCR engagement stimulates conformational changes in the CD3 or ζ chains, thereby unmasking ITAM phosphorylation sites that are subsequently phosphorylated by constitutively active Lck. In contrast, the "de novo activation" model suggests that TCR engagement transiently enhances the enzymatic activity of Lck, which then leads to ITAM phosphorylation (*6*–*8*).

The enzymatic activity of Lck is tightly controlled by differential phosphorylation of two tyrosine residues, Tyr^{394} and Tyr^{505} (*9*). The C-terminal tyrosine residue of Lck, Tyr^{505}, acts as a negative regulatory element (*10*). When phosphorylated by the cytoplasmic tyrosine kinase Csk (C-terminal Src kinase), Tyr^{505} promotes the formation of a closed, inactive conformation of Lck by interacting with the N-terminal intramolecular Src homology 2 (SH2) domain (*11*). The closed conformation is further stabilized by a physical interaction between an intramolecular SH3 domain (which precedes the SH2 domain) and a polyproline helix within the so-called linker region of Lck (*12*). The inhibitory activity of Csk is counteracted by CD45, the most abundant transmembrane tyrosine phosphatase in T cells (*13*). As a consequence of the CD45-mediated dephosphorylation of Tyr^{505}, Lck is assumed to adopt a "primed," presumably open, conformation whose role in T cell activation remains elusive. Specifically, it is still controversial whether primed Lck is enzymatically active and, if so, whether its activity is different from that of what is generally assumed to be the active form of Lck (*14*, *15*). This latter state of Lck is thought to be induced by autophosphorylation or transphosphorylation of Tyr^{394}, which is located in the activation loop of the kinase domain of Lck (*16*). Although a large number of studies underline the importance of Tyr^{394} phosphorylation for

[1]Institute of Molecular and Clinical Immunology, Otto von Guericke University, Leipziger Strasse 44, 39120 Magdeburg, Germany. [2]Leibniz Institute for Neurobiology, Brenneckestrasse 6, 39118 Magdeburg, Germany. [3]Department of Immune Control, Helmholtz Centre for Infection Research, 38124 Braunschweig, Germany. [4]Intravital Microscopy in Infection and Immunity, Helmholtz Centre for Infection Research, 38124 Braunschweig, Germany.
*These authors contributed equally to this work.
†Corresponding author. Email: andreas.mueller@med.ovgu.de (A.J.M.); luca.simeoni@med.ovgu.de (L.S.); burkhart.schraven@med.ovgu.de (B.S.)

the enzymatic activity of Lck (*15*, *17*, *18*), the individual contributions of changes in conformation and Tyr^{394} phosphorylation to Lck function are unclear.

Whereas previous studies focused mainly on the phosphorylation state of Lck to elucidate its mode of action for T cell activation, we previously used dynamic fluorescence lifetime imaging microscopy/Förster resonance energy transfer (FLIM/FRET) measurements to assess the conformational states and activity of Lck directly in live cells with a chimeric cyan fluorescent protein (CFP)–Lck–yellow fluorescent protein (YFP) biosensor (CLckY-1) (*6*). Consistent with the standby model (*5*), our steady-state measurement of Jurkat cells (that is, in the absence of TCR-mediated stimuli) revealed that a substantial proportion of endogenous Lck molecules are present in an "open" conformation that exhibits reduced FRET. However, we also demonstrated that the proportion of the CLckY-1 biosensor molecules that are closed under steady-state conditions rapidly assumes an open conformation upon stimulation of the TCR. Consistent with the biosensor data, we showed by sensitive in vitro kinase assays with endogenously produced Lck isolated from Jurkat cells or primary human T lymphocytes that T cell activation results in an increase in the enzymatic activity of Lck (*6*).

However, the low sensitivity of the CLckY-1 biosensor prevented us from dissecting how conformational changes and phosphorylation of Tyr^{394} act in concert to control Lck function. Therefore, we constructed an optimized, high-sensitivity biosensor (hereafter referred to as TqLck-V2), which was better suited for FLIM/FRET because of a near monoexponential fluorescence lifetime decay. We used the TqLck-V2 biosensor to assess the conformation of a Y394F/Y505F double mutant Lck that represents the primed form of Lck. FLIM measurements revealed that Y394F/Y505F-Lck exhibited a constitutively open conformation, which was insensitive to stimulation of the TCR. Furthermore, despite having an open conformation, the Y394F/Y505F double mutant Lck was substantially impaired in its ability to reconstitute TCR-stimulated signaling in Lck-deficient JCaM 1.6 cells. In addition, we established a standard operating procedure (SOP) for the quantitative and semiautomated immunofluorescence-based analysis of endogenous total Lck and its differentially phosphorylated forms in Jurkat cells and primary human T lymphocytes. Applying this optimized protocol, we showed that Lck underwent TCR-stimulated de novo phosphorylation of Tyr^{394} at the plasma membrane. Thus, by separately analyzing the conformational changes of Lck and the phosphorylation state of Tyr^{394} after TCR stimulation, we demonstrated that independently of its conformational state, the function of Lck critically depended on the phosphorylation of Tyr^{394}.

RESULTS

Characterization of a second-generation Lck FRET biosensor, TqLck-V2, with near-monoexponential donor fluorescence decay

In our previous study, we used an Lck biosensor, CLck-Y1, that was originally generated by Paster *et al.* (*19*). The CLck-Y1 biosensor uses the two fluorophores CFP and YFP (Fig. 1A), whereby CFP is placed N-terminally of the Lck-SH3 domain and the acceptor fluorophore YFP is placed at the C terminus of Lck. Although the CLck-Y1 biosensor and a modified version, CLck-Y2, were suitable to monitor conformational changes in Lck with FLIM, and hence, de novo activation of Lck upon T cell activation, they had the principle disadvantage that only a fraction of the CFP domains of the biosensor participate in FRET from CFP to YFP (*6*). The resulting low sensitivity of these first-generation biosensors hampered the efficacy of FLIM measurements, because each experiment required extensive mathematical calculations to extract the true FRET signal.

To circumvent this problem, we generated a second-generation biosensor in which CFP was replaced with monomeric Turquoise2 (Tq), which has a monoexponential fluorescence decay (*20*), and YFP was replaced with monomeric Venus (V) (*21*). In addition, we changed the location of the donor fluorophore Tq within the Lck backbone and positioned it between the SH3 and SH2 domains of Lck (Fig. 1A), because Paster *et al.* showed that a biosensor carrying the donor fluorophore at this particular position (CLck-Y2) reconstituted TCR-mediated signaling better than did the CLck-Y1 biosensor (*19*). We first compared global tyrosine phosphorylation in unstimulated or TCR-stimulated cells expressing either CLck-Y1 or TqLck-V2 (fig. S1A). On the basis of the new fluorophores and the altered position of the donor fluorophore in comparison to the first-generation CLck-Y1 and CLck-Y2 biosensors, we termed the second-generation biosensor TqLck-V2 (Fig. 1, A and B). We also confirmed the monoexponential fluorescence decay of the new FRET donor (Fig. 1C), which corresponded well with the biophysical properties found by Goedhart *et al.* (*20*) for both the old and new fluorophores (table S1). We found that the pattern of TCR-stimulated global tyrosine phosphorylation in JCaM 1.6 cells expressing TqLck-V2 was very similar, if not identical, to the pattern of the previously published first-generation biosensor CLck-Y2 (fig. S1A; for comparison, CLck-Y1 is also shown). Lck-deficient JCaM 1.6 cells transiently expressing the *tqLck-V2* construct exhibited, in response to antibody-mediated TCR stimulation, ERK phosphorylation and Ca^{2+} mobilization (Fig. 1, D and E) responses that were comparable to those exhibited by cells expressing either of the first-generation biosensors. Thus, these data indicate that TqLck-V2 is functional in JCaM 1.6 cells.

The TCR-induced increases in phosphorylated ERK (pERK) abundance and Ca^{2+} flux in JCaM 1.6 cells expressing the biosensor constructs were consistently reduced compared to those in wild-type JE6 cells. However, the inability of TqLck-V2 to fully rescue signaling in Lck-deficient JCaM 1.6 cells was not due to aberrant functionality of the second-generation biosensor, because we observed the same phenomenon when we expressed a C-terminally single-tagged *lck-YFP* gene construct in these cells (fig. S1, B to D). In-depth analysis rather showed that the weaker response of the population of transfected cells was mainly because JCaM 1.6 transfectants that produced very high amounts of the biosensor (or of the single YFP-tagged Lck variant) became unresponsive to TCR-mediated stimuli (fig. S1, B to D). Only those cells that produced intermediate amounts of the Lck constructs (even nontagged Lck) were capable of activating ERK in response to TCR stimulation, which resulted in a weaker signaling response when the whole cell population was analyzed (fig. S1A). For all subsequent analyses, we therefore gated on cells that produced intermediate amounts of the various biosensor molecules.

We next performed FLIM measurements with TqLck-V2. To this end, TCR-stimulated JCaM 1.6 cells expressing intermediate amounts of TqLck-V2 were selected and subjected to FLIM/FRET analysis. The conformational opening of TqLck-V2 upon TCR stimulation, but not that of the first-generation biosensor, was readily observable by measuring the mean fluorescence lifetimes of the reporter (Fig. 1F), which was easier to perform than the extraction of pre-exponential factors that would have been necessary if the first-generation biosensors were used (*6*). We also found that there was a more substantial

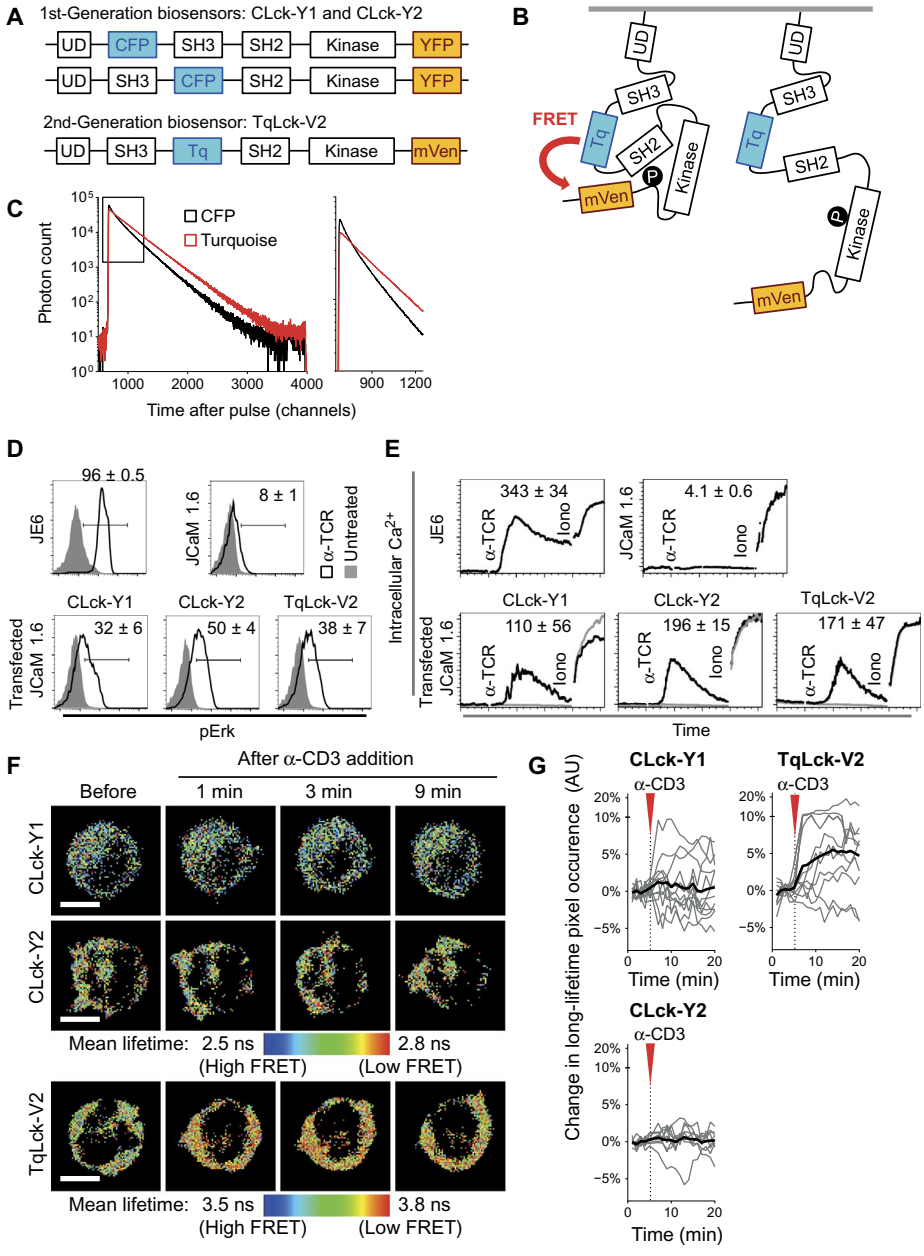

Fig. 1. Design and validation of a highly sensitive second-generation Lck FRET biosensor, TqLck-V2. (**A**) Comparison of first-generation (CLck-Y1 and CLck-Y2) and second-generation (TqLck-V2) biosensor domain structures. mVen, mVenus; UD, unique domain. (**B**) Schematic representation of the conformational changes that result in FRET changes in the biosensor on the basis of the model for Src family kinase activation and Lck stabilization (*11*, *41*, *42*). (**C**) Fluorescence decay kinetics of the FRET donors alone. Data are representative of more than 50 cells pooled from >10 independent experiments. (**D**) Comparison of ERK phosphorylation induction in response to TCR stimulation measured in JE6.1 Jurkat (JE6) cells and Lck-deficient JCaM 1.6 cells expressing the indicated first- and second-generation biosensor constructs. Events were gated on yellow fluorescence (YFP or mVenus, respectively)–intermediate cells as described in fig. S1. Mean values ± SD of pERK-positive cell frequencies from four independent measurements are indicated within the graphs. (**E**) JE6, untransfected JCaM 1.6, and JCaM 1.6 cells expressing the indicated biosensors were examined for Ca^{2+} flux upon stimulation of the TCR. Traces indicated by black curves (except for the JE6 control) were from cells that were gated as described in (D). Iono, ionomycin (positive control); gray curve, gated on untransfected cells. Total measurement duration was 512 s. Mean values ± SD of the Ca^{2+} signal increase from three independent measurements are indicated within the graphs. (**F**) Examples of the mean fluorescence lifetime changes in JCaM 1.6 cells transfected with constructs encoding the indicated biosensors upon TCR stimulation. Scale bar, 5 μm. Data are representative of at least nine cells measured in at least three independent experiments. (**G**) Quantification of the data represented in (F). Relative increase in long lifetimes [shown as yellow and red pixels in (F)] for individual cells during TCR stimulation. Gray curves represent the individual cells, whereas the black curve represents the average. AU, arbitrary units.

increase in pixels with a high mean fluorescence lifetime (and hence loss of FRET) upon TCR stimulation of cells expressing TqLck-V2 compared to that in cells expressing either CLck-Y1 or CLck-Y2 (Fig. 1G). Thus, TqLck-V2 behaves similarly to Lck in T cells, and, because of its higher sensitivity to changes in FRET, it is better suited than CLck-Y1 or CLck-Y2 for sensitive FLIM measurements.

Role of Lck conformation and Tyr^{394} phosphorylation for TCR-mediated signaling

To date, it has been unclear whether conformational opening of Lck alone is sufficient to activate T cells. To address this question, we generated three individual mutants of the TqLck-V2 biosensor to reflect particular conformational states of Lck (*14*): the Y394F mutant (a constitutively closed form of Lck), the Y505F mutant (a constitutively open form of Lck), and the Y394F/Y505F double mutant (which corresponds to the primed form of Lck). In particular, we were interested in investigating the Y394F/Y505F mutant, because both functional and structural data on the nonphosphorylated (primed) form of Lck are largely incomplete. We measured the average fluorescence lifetimes of the three reporter mutants in the absence of TCR stimulation (steady-state conditions) (Fig. 2, A and B). Consistent with previous findings (*19*), under steady-state conditions, the Y394F mutant showed a constitutively closed conformation with high FRET with a mean fluorescence lifetime of the donor fluorophore of 3.55 ns, whereas the Y505F mutant had a constitutively open conformation and exhibited a mean lifetime of 3.80 ns. Furthermore, and in contrast to the wild-type biosensor, both the Y394F and the Y505F mutants did not exhibit conformational changes upon TCR stimulation (Fig. 2, C to E). This suggests that these two biosensor mutants are present in JCaM 1.6 in conformations that are unresponsive to TCR-mediated signals. Although this finding was anticipated for the constitutively open Y505F mutant, the observation that the Y394F did not alter its conformation upon TCR stimulation was somewhat unexpected, because in principle it would have been for TCR stimulation to induce the dephosphorylation of Tyr^{505}, thereby generating the nonphosphorylated, primed form of Lck.

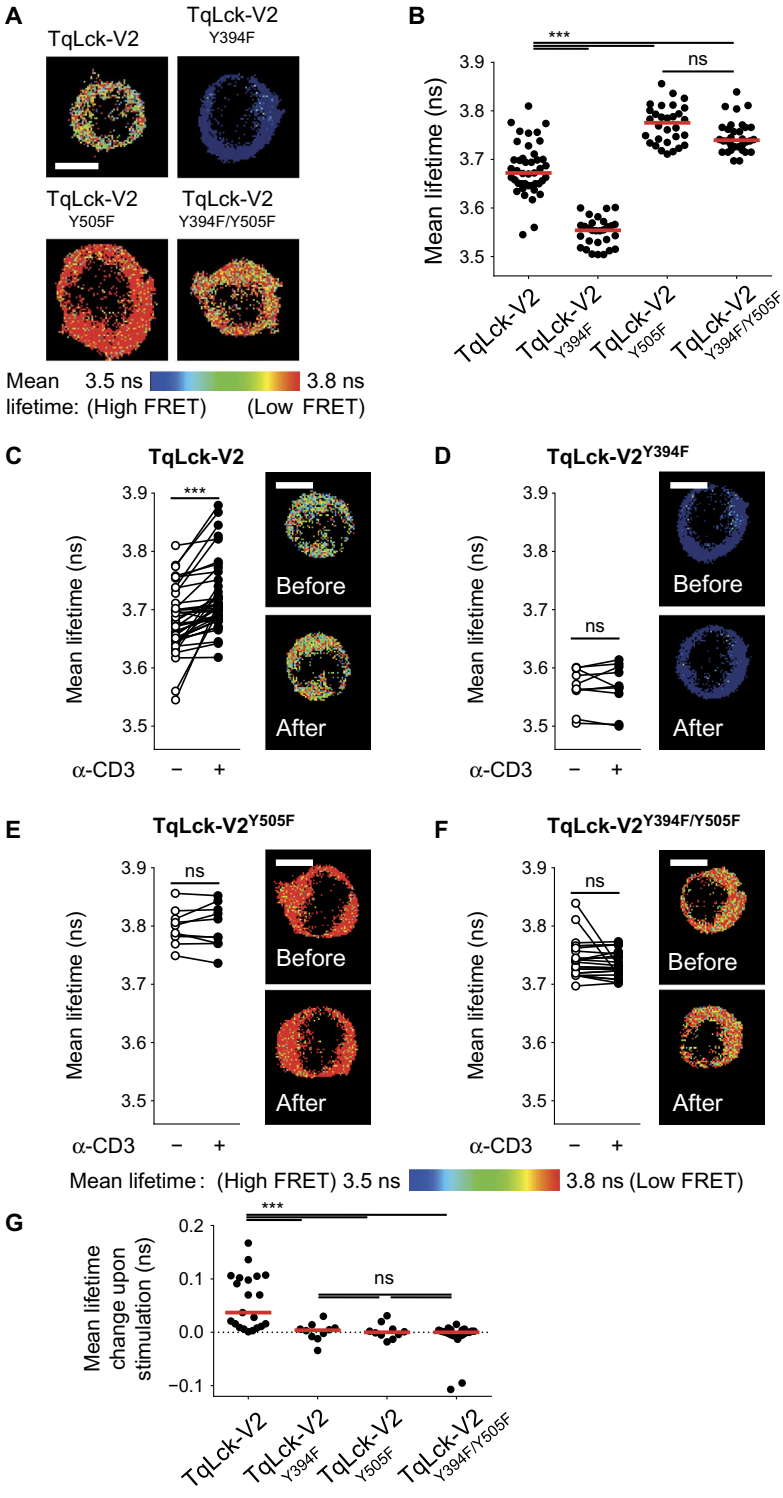

Fig. 2. FLIM analysis of the wild-type and tyrosine mutant TqLck-V2 biosensors. (**A**) Example of average fluorescence lifetime maps of wild-type (WT), Y394F, Y505F, and double mutant biosensor in JCaM 1.6 cells under steady-state conditions. Images are representative of at least five independent experiments. Scale bar, 5 μm. (**B**) Quantitative analysis of mean fluorescence lifetimes under steady state. Each dot represents a single transfected cell; horizontal bars denote the mean; ns, not significant; ***P < 0.001. (**C** to **F**) Fluorescence lifetime measurement of JCaM 1.6 cells transfected with plasmids encoding the WT (C), Y394F (D), Y505F (E), or double mutant Y394F/Y505F constructs of the TqLck-V2 biosensor (F) before [open circles, as shown in (B)] and after (closed circles) TCR stimulation. Symbols connected with a line represent the same cell before and after treatment. Scale bar, 5 μm; ***P < 0.001. (**G**) Change in mean lifetime upon TCR stimulation for the cells analyzed in (C) to (F). Horizontal bars denote the median; ***P < 0.001. Data in (B) to (G) are pooled from at least five independent experiments.

Instead, our data suggest that in cells expressing the Y394F mutant Lck, TCR stimulation does not result in substantial dephosphorylation of Tyr^{505}.

In the absence of TCR stimulation, the Y394F/Y505F mutant TqLck-V2 had a lifetime that was very close to the lifetime of the constitutively open Y505F mutant. This finding suggests that, similar to the Y505F mutant, the Y394F/Y505F mutant is also present in a constitutively open conformation. We next assessed whether TCR stimulation would induce a conformational change in the double mutant biosensor. However, whereas the wild-type biosensor adopted an open conformation upon TCR stimulation (Fig. 2C), the conformation of the Y394F/Y505F mutant did not change (Fig. 2, F and G). Hence, similar to Y505F, the Y394F/Y505F double mutant adopted a constitutively open conformation that did not change upon TCR stimulation. To exclude the possibility that the tyrosine-to-phenylalanine mutation locked the biosensor into its particular conformation, we repeated the FLIM experiments with cells expressing either the Y394A single mutant or the Y394A/Y505F double mutant, and we generated essentially identical data (fig. S2). These findings suggest that the closed conformation adopted by Lck variants with a mutation of Tyr^{394} was not caused specifically by the presence of phenylalanine at position 394.

Conflicting data have been published regarding the functional properties of the nonphosphorylated, primed form of Lck. Although a report suggested that the enzymatic activity of primed Lck is only slightly less than that of wild-type Lck (*14*), in vitro kinase assays with the same mutant showed that its kinase activity more closely resembles that of the Y394F mutant (*15*). To address whether the primed form of Lck reconstituted T cell activation upon TCR stimulation, we performed experiments with JCaM 1.6 cells expressing the wild-type TqLck-V2 biosensor or its Y505F, Y394F, or Y394F/Y505F mutants in which we assessed the capability of the cells to respond to TCR stimulation (Fig. 3). We first confirmed that the biosensors were present at equivalent abundances by measuring the fluorescence intensities of JCam1.6 cells expressing the individual biosensors (fig. S3). We found that the wild-type biosensor and the constitutively open Y505F mutant rescued

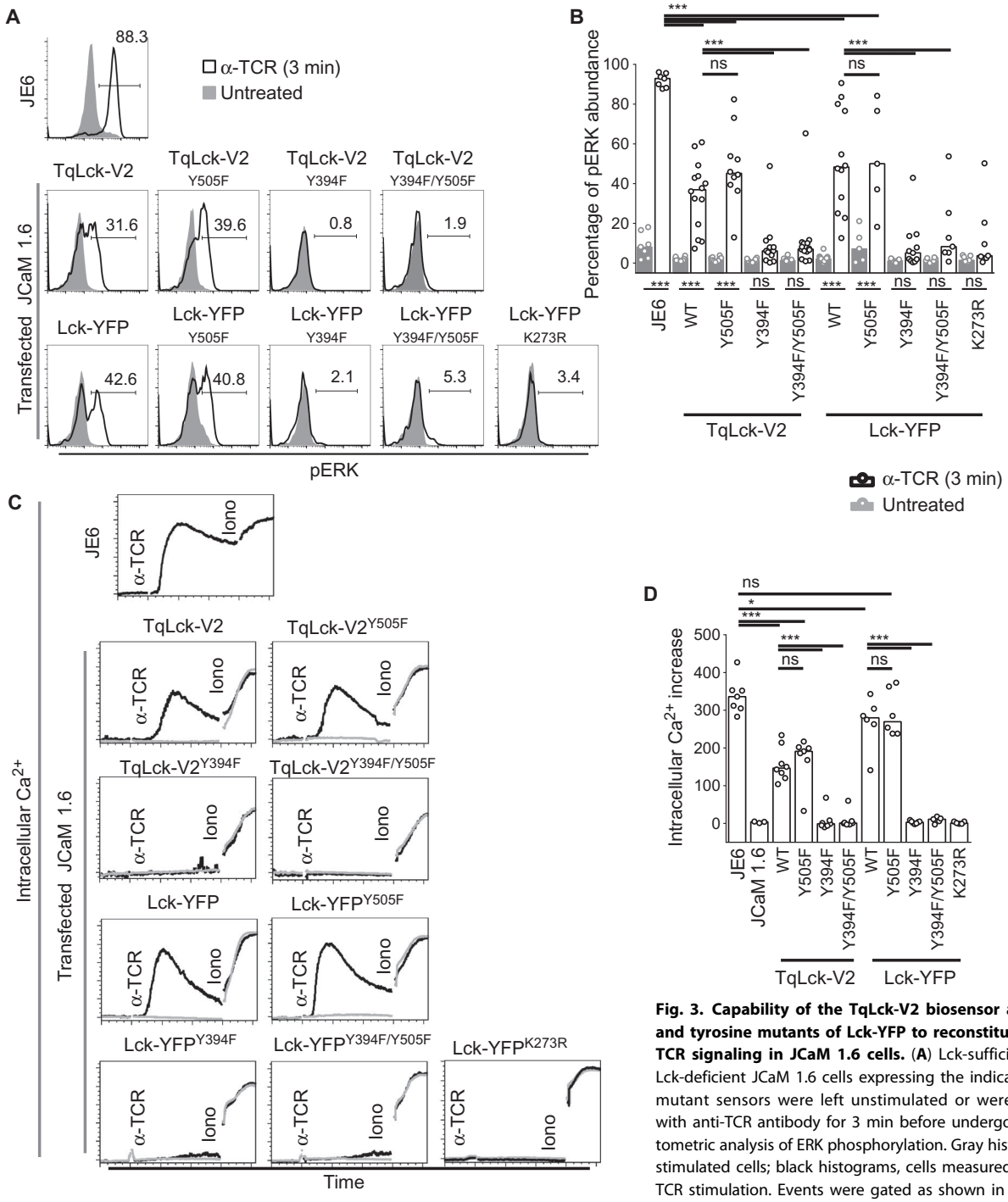

Fig. 3. Capability of the TqLck-V2 biosensor and the WT and tyrosine mutants of Lck-YFP to reconstitute proximal TCR signaling in JCaM 1.6 cells. (**A**) Lck-sufficient JE6 and Lck-deficient JCaM 1.6 cells expressing the indicated WT and mutant sensors were left unstimulated or were stimulated with anti-TCR antibody for 3 min before undergoing flow cytometric analysis of ERK phosphorylation. Gray histograms, unstimulated cells; black histograms, cells measured 3 min after TCR stimulation. Events were gated as shown in fig. S1. Data are representative of at least five independent experiments. (**B**) Percentages of pERK-positive cells before (gray) and after (black) TCR stimulation. Bars, average values; each symbol represents one experimental condition in an independent experiment; ***$P < 0.001$. (**C**) JE6 and JCaM 1.6 cells expressing the indicated constructs were stimulated through the TCR, and Ca^{2+} flux measurements were made as described in Fig. 1E. Black curves (except for the JE6 control) were from cells gated as described in (A); gray curves were from cells gated on untransfected cells. Total measurement duration was for 512 s. Data are representative of at least three independent experiments. (**D**) Measurement of Ca^{2+} increases after TCR stimulation of JE6 cells and of JCaM 1.6 cells expressing the indicated constructs. Bars represent averages; each symbol represents a single experimental condition in an independent experiment; *$P < 0.05$; ***$P < 0.001$.

ERK phosphorylation (Fig. 3, A and B), Ca^{2+} flux (Fig. 3, C and D), and the increased cell surface abundance of the activation marker CD69 (fig. S4) upon TCR stimulation to similar extents, whereas the closed mutant Y394F failed to rescue signaling. Moreover, although exhibiting an open conformation (similar to that of the Y505F mutant), the Y394F/Y505F double mutant was also unable to mediate TCR-proximal signaling,

suggesting that this mutant functionally behaves similarly to Y394F. Note that we reproduced these findings in experiments with single-tagged Lck-YFP versions of the mutants, which indicate that the insertion of the FRET donor domain between the SH3 and SH2 domains did not alter the signaling properties of the biosensor molecules. Together, our data suggest that the forced opening of the conformation of Lck alone (as occurs in the Y394F/Y505F mutant) does not facilitate TCR-proximal signaling in T cells. Rather, it appears that, in addition to undergoing a conformational change, de novo phosphorylation of Tyr^{394} is required for Lck to initiate signaling upon TCR stimulation.

An optimized protocol for Lck immunofluorescence staining

The apparent dependency of TCR-proximal signaling on the phosphorylation of Tyr^{394} prompted us to analyze the phosphorylation status of Lck at a single-cell level. Whether de novo phosphorylation of Lck occurs upon stimulation of the TCR is still debated (*5*, *7*). In addition, much of the conflicting data regarding this issue originate from the lack of a standardized experimental protocol. Thus, we sought to set up an SOP that enables a quantitative, single cell–based approach for the confocal analysis of total Lck and its phosphorylated forms. We took advantage of JCaM 1.6 cells stably transfected with plasmid encoding the TqLck-V2 construct (fig. S5A). We observed the characteristic localization of Lck at the plasma membrane and in an intracellular vesicular pool, which was also previously described (fig. S5B) (*22*, *23*). We then stained wild-type Lck in JE6 cells treated with a panel of different fixative combinations to determine the condition that best recapitulated the distribution of fluorescently tagged Lck in live cells (fig. S5, C to E). In brief, we found that fixation of the cells with a solution of 1% paraformaldehyde (PFA) and 0.02% glutaraldehyde (GA) resulted in optimal staining of Lck both in the intracellular vesicular compartment and in the plasma membrane, whereas nonspecific staining was kept to a minimum (fig. S5). Staining of total Lck using the SOP resulted in a pattern that overlapped completely with fluorescently labeled Lck in JCaM 1.6 cells stably transfected with plasmid encoding the TqLck-V2 construct (Fig. 4, A and B). In addition, the SOP permitted the detection of a strong signal in cells stained with phosphospecific antibodies that detect $pTyr^{394}$ and $pTyr^{505}$ of Lck (fig. S5, F and G). Thus, this SOP was used for all subsequent analyses of Lck phosphorylation.

Although it does not enable the analysis of molecular events at a single-cell level, Western blotting has been the gold standard to date for investigating TCR-proximal signaling events. We thus sought to compare the changes in Lck Tyr^{394} and Tyr^{505} phosphorylation observed by Western blotting analysis with immunofluorescence analysis according to the SOP. To this end, JE6 cells expressing endogenously *lck* and primary human T cells were treated with 10 μM 4-amino-5-(4-chlorophenyl)-7-(dimethylethyl)pyrazolo[3,4-d]pyrimidine (PP2; an Src family kinase inhibitor) for 30 min (*24*) or with 1 mM pervanadate (PV; a phosphatase inhibitor) for 2 min (*25*), which should induce minimal (PP2) or maximal (PV) phosphorylation of Lck, respectively. Subsequently, the cells were subjected either to confocal microscopy with the optimized fixation and staining protocol (Fig. 4, C to F) or to Western blotting analysis with an anti–phospho-Lck antibody (Fig. 4, G and H). The changes in Lck phosphorylation upon treatment with PP2 or PV treatment that were observed by Western blotting analysis (Fig. 4H) were fully recapitulated by immunofluorescence microscopy (Fig. 4, D and F). This suggests that the optimized staining protocol is a suitable tool for the quantitative analysis of Lck phosphorylation.

Increased Lck Tyr^{394} phosphorylation at the plasma membrane upon TCR stimulation

Our earlier data showed that the two Lck mutants Y394F (constitutively closed) and Y394F/Y505F (constitutively open) in which Tyr^{394} cannot be phosphorylated are unable to reconstitute TCR-mediated signaling. This finding suggested a requirement for de novo phosphorylation of Tyr^{394} upon TCR stimulation. Consistent with this hypothesis, immunofluorescence staining of JE6 cells through the SOP showed a substantial increase in the phosphorylation of Tyr^{394} (and Tyr^{505}) upon TCR stimulation (Fig. 5, A and B). Note that the relative increase in phosphorylation of the regulatory tyrosines was also observed in human primary T cells (Fig. 5, C and D), which excludes the possibility that augmentation of Tyr^{394} and Tyr^{505} phosphorylation upon TCR stimulation is a particular property of the JE6 cells. Thus, T cell activation induced de novo phosphorylation of Tyr^{394} (and Tyr^{505}), and this event was required to initiate receptor-proximal signaling upon TCR stimulation.

Next, we sought to test whether the wild-type TqLck-V2 biosensor and the constitutively open Y505F mutant, respectively, would also show de novo Tyr^{394} phosphorylation upon TCR triggering. Because only a small percentage of cells were found to express the biosensor construct at quantities that enabled the induction of ERK phosphorylation (fig. S1C), we adapted the SOP for flow cytometric analysis (Fig. 6), which has already been successfully used to study the phosphorylation of Tyr^{394} and Tyr^{505} (*26*). By gating only on cells displaying a physiological basal content of $pTyr^{394}$ and an intermediate biosensor fluorescence (Fig. 6, A to C), we found that the ratio of the $pTyr^{394}$ signal to biosensor content (which was determined by yellow fluorescence) increased upon TCR stimulation (Fig. 6, D and E). This suggests that not only endogenously expressed *lck*, but also the transiently expressed biosensor construct, is de novo phosphorylated on Tyr^{394} upon TCR stimulation. The flow cytometric protocol also enabled us to assess the Y394F biosensor mutant in more detail. We showed earlier that the Y394F mutant does not undergo a conformational change upon TCR stimulation. As suggested earlier, this is due to the fact that Tyr^{505} is not subjected to dephosphorylation upon TCR stimulation (fig. S7).

An important advantage of an image-based phosphorylation analysis over Western blotting is the possibility to determine the subcellular localization of differentially phosphorylated proteins and to analyze the distribution of the respective forms of the proteins at a cellular level. This is of special interest because Lck activation could be different in the membranous versus the intracellular pool. Moreover, a redistribution of preactivated Lck has been proposed as a mode of action for the Lck-mediated initiation of TCR-proximal signaling (*5*, *27*). Finally, to date, it is not known how the phosphorylation status of Lck affects its subcellular localization.

To assess these questions, we analyzed the subcellular localization of $pTyr^{394}$ and $pTyr^{505}$ after TCR stimulation. We used an adapted version of the DISCit approach, which was originally developed for analyzing cellular dynamics in vivo (*28*). In brief, cells were automatically segmented into a plasma membrane and a non–plasma membrane compartment (which included the intracellular vesicular pool of Lck). Subsequently, the fluorescence intensities of the two compartments of all cells were converted into a cytometry data set and analyzed at a single-cell level with cytometry software (Fig. 7A). For the analysis of the changes in pLck abundance and distribution upon TCR stimulation, the fluorescence intensities were normalized to the untreated values of the respective compartments. This enabled us to investigate changes in

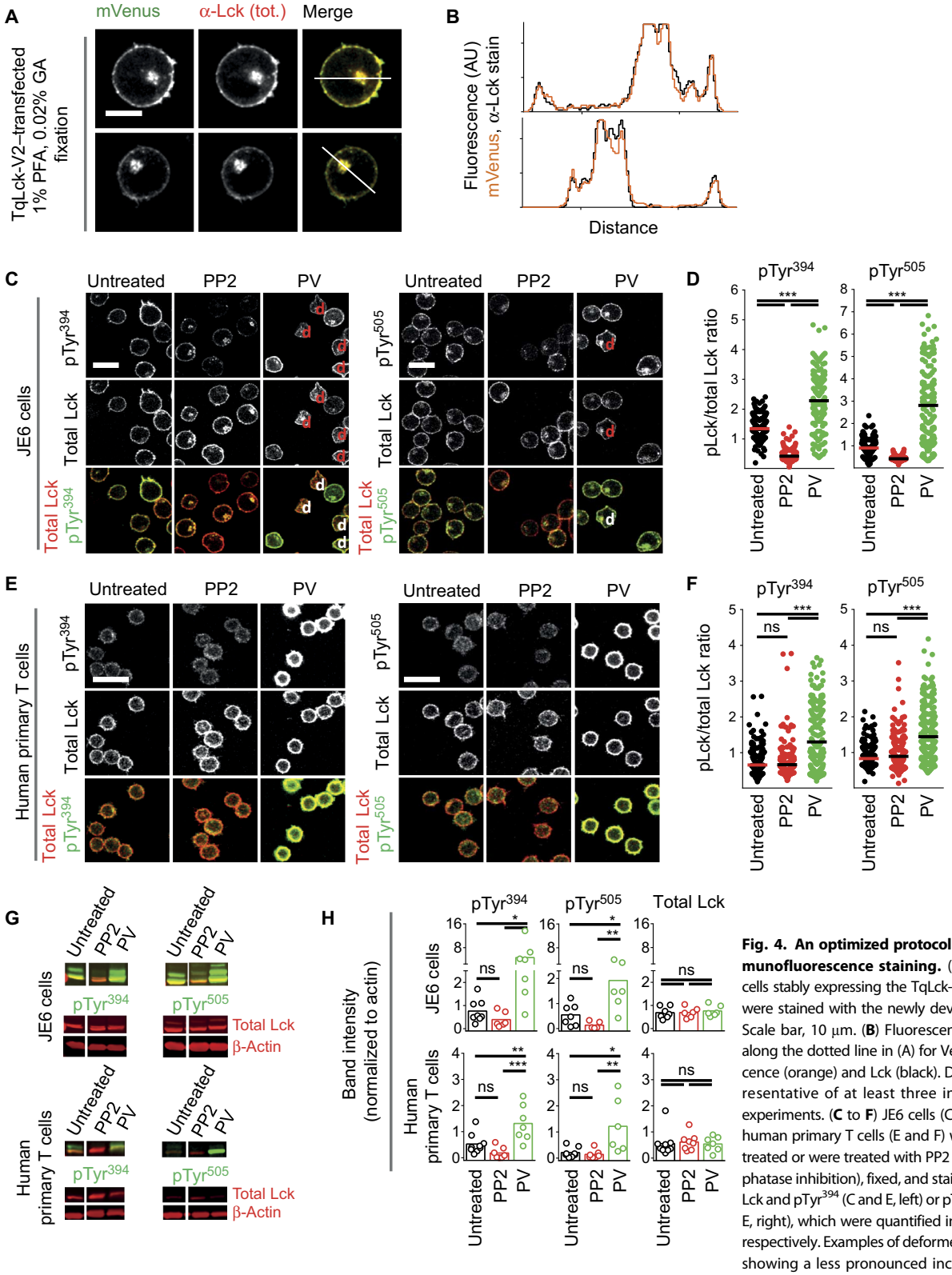

Fig. 4. An optimized protocol for Lck immunofluorescence staining. (**A**) JCaM 1.6 cells stably expressing the TqLck-V2 construct were stained with the newly developed SOP. Scale bar, 10 μm. (**B**) Fluorescence intensity along the dotted line in (A) for Venus fluorescence (orange) and Lck (black). Data are representative of at least three independent experiments. (**C** to **F**) JE6 cells (C and D) and human primary T cells (E and F) were left untreated or were treated with PP2 or PV (phosphatase inhibition), fixed, and stained for total Lck and pTyr^{394} (C and E, left) or pTyr^{505} (C and E, right), which were quantified in (D) and (F), respectively. Examples of deformed dead cells showing a less pronounced increase in the pTyr signal after PV treatment are labeled with "d." (C and E) Images are representative of three independent experiments. Scale bar, 20 μm. (D and F) Single-cell analysis of Tyr^{394} and Tyr^{505} phosphorylation relative to total Lck from three compiled independent experiments. Each dot represents an individual JE6 (D) or human primary T cell (F). Horizontal bars, mean; ***$P < 0.001$. (**G**) Western blotting analysis of phosphorylated Lck (pLck) (green) and total Lck (red) in JE6 cells (top) and primary human T cells (bottom) that were left untreated or were treated with PP2 or PV. (**H**) Quantification of Western blotting band intensities. Each dot represents one independent Western blot. Data are pooled from at least six independent Western blots. Values were normalized to the β-actin loading control. *$P < 0.05$; **$P < 0.01$; ***$P < 0.001$.

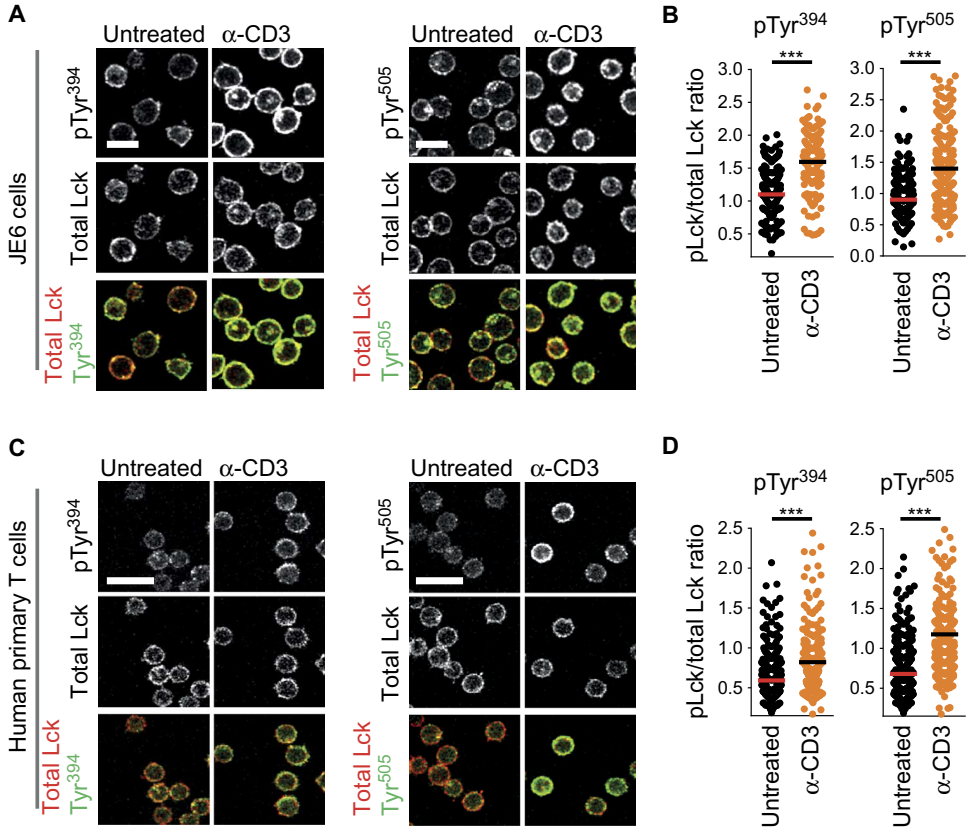

Fig. 5. De novo Tyr^{394} and Tyr^{505} phosphorylation in JE6 and human primary T cells upon TCR stimulation. (**A** to **D**) JE6 cells (A and B) and human primary T cells (C and D) were left untreated or were treated for 2 min with anti-CD3 antibody to cross-link the TCR and then were fixed and stained for total Lck and pTyr^{394} (A and C, left) or pTyr^{505} (A and C, right), respectively. (A and C) Images are representative of three independent experiments, which are quantified in (B) and (D), respectively. Scale bar, 20 μm. (B and D) Single-cell analysis of Lck-pTyr^{394} and Lck-pTyr^{505} abundance normalized to that of total Lck upon TCR stimulation of cells from three pooled independent experiments. Each dot represents an individual JE6 (B) or human primary T cell (D). ***$P < 0.001$. Note that the anti-CD3 antibody [mouse IgG1 (immunoglobulin G1), clone UCHT1] used for TCR stimulation was not recognized by the secondary anti-mouse IgG2b antibody that was used to detect the primary anti-total Lck antibody (see fig. S6).

DISCUSSION

Lck is the primary tyrosine kinase that propagates TCR-mediated signals in the cell; however, it is still debated how Lck initiates the phosphorylation of its immediate downstream substrates, the ITAMs of the TCR-CD3-ζ complex. Using a FRET-based Lck biosensor (CLckY-1), we previously demonstrated that about 20% of the Lck molecules in primary human T cells or the JE6 cell line rapidly undergo a conformational change upon T cell activation (*6*). Moreover, we showed that this conformational change preferentially occurs at the contact site between T cells and APCs, thus providing evidence that local de novo opening of Lck upon TCR stimulation is linked with the phosphorylation of the ITAMs. Together, our previous data demonstrated that the Lck biosensor is a tool that enables study of the principal biological properties of Lck.

However, our first-generation CFP-YFP–based CLckY-1 biosensor had the major disadvantage of having low FRET efficiency because of the biophysical properties of the CFP-YFP FRET pair. The multiexponential fluorescence decay of CFP even when not coupled to any FRET acceptor results in an even more complex behavior of CFP-YFP FRET, with at least three lifetime components to fit the measured data (*29*–*32*). Only one of these lifetime components is involved in the FRET process, which contributes to less than 30% of the total decay function (*33*). In contrast to that of CFP, the fluorescence decay of mTurquoise2 is nearly monoexponential (Fig. 1C), and hence, the respective FRET pairs can be analyzed with two lifetimes (*20*), whereby the lifetime involved in FRET contributes to more than 90% of the decay function. Additionally, the higher quantum yield of mTurquoise2 and lower photobleaching enable the reduction of the intensity of sample illumination compared to that for CFP-based FRET constructs, thus minimizing light-dependent side effects, such as reactive oxygen species production (table S1). Here, we showed that, similar to CLckY-1, CLckY2, and C-terminally YFP-tagged Lck lacking an intramolecular FRET donor domain, the optimized second-generation Lck biosensor TqLck-V2 rescued TCR-mediated signaling in JCaM 1.6 cells. Moreover, FLIM measurements with TqLck-V2 corroborated our previous findings that TCR stimulation induces a rapid conformational change in Lck.

The higher sensitivity of the second-generation Lck biosensor enabled a detailed study of the biophysical properties of tyrosine mutants of Lck, such as Y394F (which represents a constitutively inactive Lck) and Y505F (which represents a fully activated Lck), which so far have been mostly characterized by biochemical and functional experiments. FLIM measurements of the two single mutants demonstrated that they both occur in conformations that do not change

the pLck signal (Fig. 7B, *y* axis) as well as subcellular distribution of Lck phosphorylation (*x* axis).

We found that TCR-mediated Lck phosphorylation of Tyr^{394} occurred mainly at the plasma membrane of JE6 cells, whereas phosphorylation of Tyr^{505} was observed preferentially in the nonmembrane compartment, which contained the intracellular pool (Fig. 7C). The preferential modification of Tyr^{394} at the plasma membrane upon TCR stimulation is consistent with our previous observations that the most extensive opening of Lck (as determined by FLIM) occurred at the T cell–antigen-presenting cell (APC) interface in JE6 cells (*6*). In contrast to what occurred in JE6 cells, primary human T cells exhibited phosphorylation of both Tyr^{394} and Tyr^{505} at the plasma membrane (Fig. 7D). This finding suggests that depending on the cell type and its (pre)activation status, phosphorylation of Lck on Tyr^{505} might take place in distinct subcellular compartments. Nevertheless, our immunofluorescence analysis showed the de novo phosphorylation of Lck upon TCR stimulation and thus supports the notion that this event is crucial for the regulation of the conformation of Lck and for the initiation of TCR-proximal signaling upon antigen encounter.

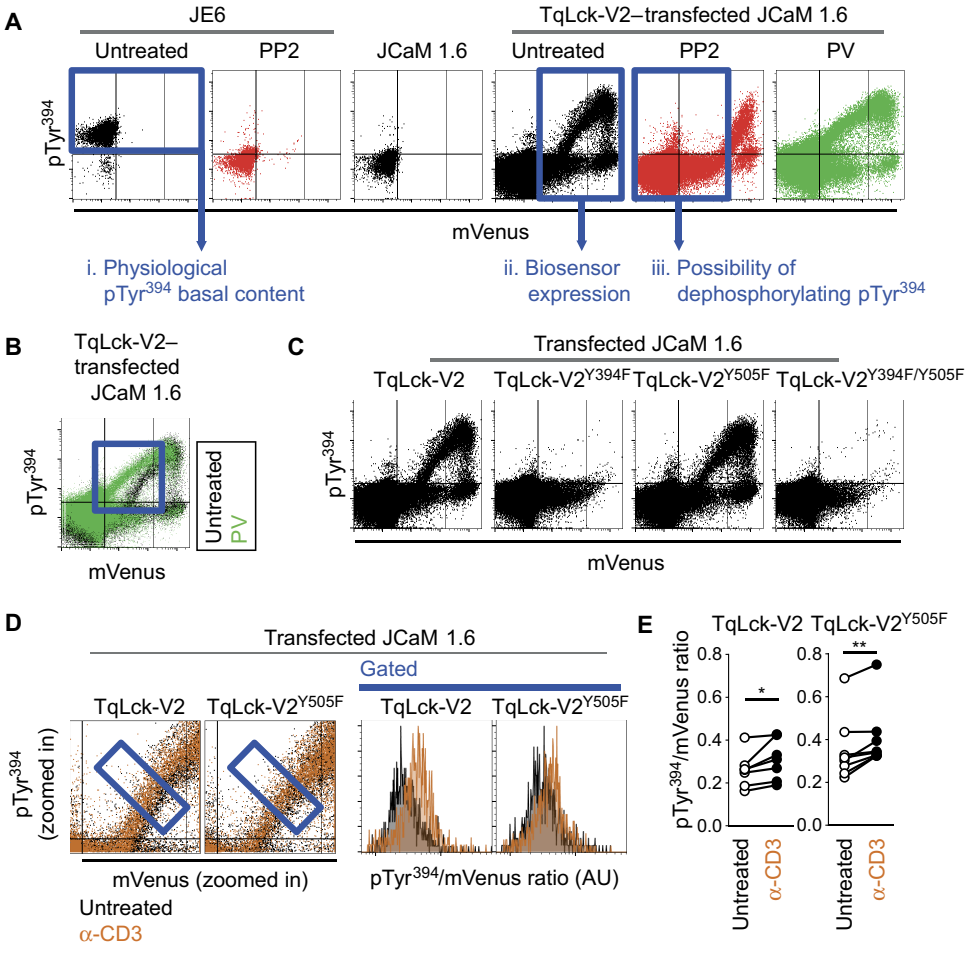

Fig. 6. De novo phosphorylation of Tyr^{394} occurs in JCaM 1.6 cells transfected with constructs encoding WT TqLck-V2 or the constitutively open TqLck-V2^{Y505F} mutant biosensor. JE6 and JCaM 1.6 cells transfected with plasmids encoding the various TqLck-V2 constructs were stained according to the SOP for pTyr^{394}, treated as indicated by PV, PP2, or TCR cross-linking or left untreated, and then were analyzed by flow cytometry. (**A**) Gating strategy applied to identify the subset of WT biosensor transfectants that showed (i) a basal physiological abundance of pTyr^{394} comparable to that of JE6 cells, (ii) biosensor fluorescence, and (iii) complete dephosphorylation upon PP2 treatment. (**B**) Comparison of pTyr^{394} and biosensor fluorescence in untreated (black) and PV-treated (green) JCaM 1.6 cells transfected with the TqLck-V2 expression construct. The subset of cells identified in (A) is boxed. (**C**) JCaM 1.6 cells transfected with the indicated biosensor variants were analyzed by flow cytometry to detect pTyr^{394} signal. Data in (A) to (C) are representative of at least six independent experiments. (**D**) Gating strategy to identify changes in the pTyr^{394}-to-Venus signal ratio in the TqLck-V2 WT biosensor and the TqLck-V2^{Y505F} mutant in untreated cells (black) and upon treatment with anti-TCR antibody (orange). Data are representative of seven independent experiments. (**E**) Quantitative analysis of the pTyr^{394}-to-Venus fluorescence ratio in transfected JCaM 1.6 cells expressing the indicated biosensors that were left untreated (open symbols) or were treated with anti-TCR antibody (closed symbols) and gated as shown in (D). Lines connect data points obtained from the same transfection and data pooled from seven independent experiments are shown; *$P < 0.05$; **$P < 0.01$.

upon TCR-mediated stimulation. This locked conformation was not a result of having specifically phenylalanine at position 394 in the mutants, because a tyrosine-to-alanine mutation had the same effect on the biosensor. With regard to Y505F, our data were somewhat expected because the C-terminal part of this mutant cannot fold back to the internal SH2 domain. In contrast, the observation that the Y394F mutant did not undergo any conformational change in response to TCR stimulation was unexpected, because the mutant should in principle retain its capability to open, for example, if the negative regulatory tyrosine of Lck became dephosphorylated upon TCR stimulation. When both Tyr^{394} and Tyr^{505} were mutated (Y394F/Y505F mutant), the nonphosphorylated form of Lck adopted an open conformation, similar to that of Y505F. Thus, the FLIM measurements with the Y394F biosensor mutant suggest that Tyr^{505} is not subjected to (further) dephosphorylation upon T cell activation, which we confirmed by measuring pTyr^{505} by flow cytometry. Consistent with this assumption, immunofluorescence analyses using the optimized staining protocol revealed an increase in the phosphorylation of both Tyr^{394} and Tyr^{505} in activated T cells.

In human resting T cells, about 50% of the Lck molecules are present in the so-called primed form, which is not phosphorylated on either Tyr^{394} or Tyr^{505} (*5*). The functional properties of this form of Lck are still not well defined. The availability of the second-generation TqLck-V2 biosensor enabled us to assess the structural properties of nonphosphorylated, primed Lck both under steady-state conditions and after TCR stimulation. FLIM measurements revealed that the Y394F/Y505F Lck biosensor mutant exhibits a more open conformation under steady-state conditions (in the absence of TCR stimulation) than has the wild-type molecule, similar to that of the constitutively open Y505F mutant. On the basis of this observation and of a study suggesting that the enzymatic activity of nonphosphorylated, primed Lck is similar to that of the pTyr^{394}/pTyr^{505} double-phosphorylated form of Lck (*14*), we had expected that the Y394F/Y505F biosensor mutant would rescue TCR-mediated signaling in JE6 cells. However, functional readouts (such as intracellular Ca^{2+} flux, activation of ERK, and increased CD69 abundance) showed that the double mutant of TqLck-V2 was functionally inactive to an extent that was comparable with the Y394F biosensor. Thus, by separating the conformation of Lck from its phosphorylation status, we showed that the conformational opening of Lck is not sufficient to induce T cell activation. Rather, in addition to the conformational opening of Lck, Tyr^{394} must undergo phosphorylation. Only when both events occur in parallel is Lck capable of facilitating T cell signaling. The notion of distinct roles for conformational opening and Lck kinase activity is supported by an elegant superresolution microscopy study that showed that the opening of Lck controls the formation of functionally distinct signaling microclusters upon TCR stimulation. The formation of these microclusters occurs independently of the kinase activity of Lck (*34*).

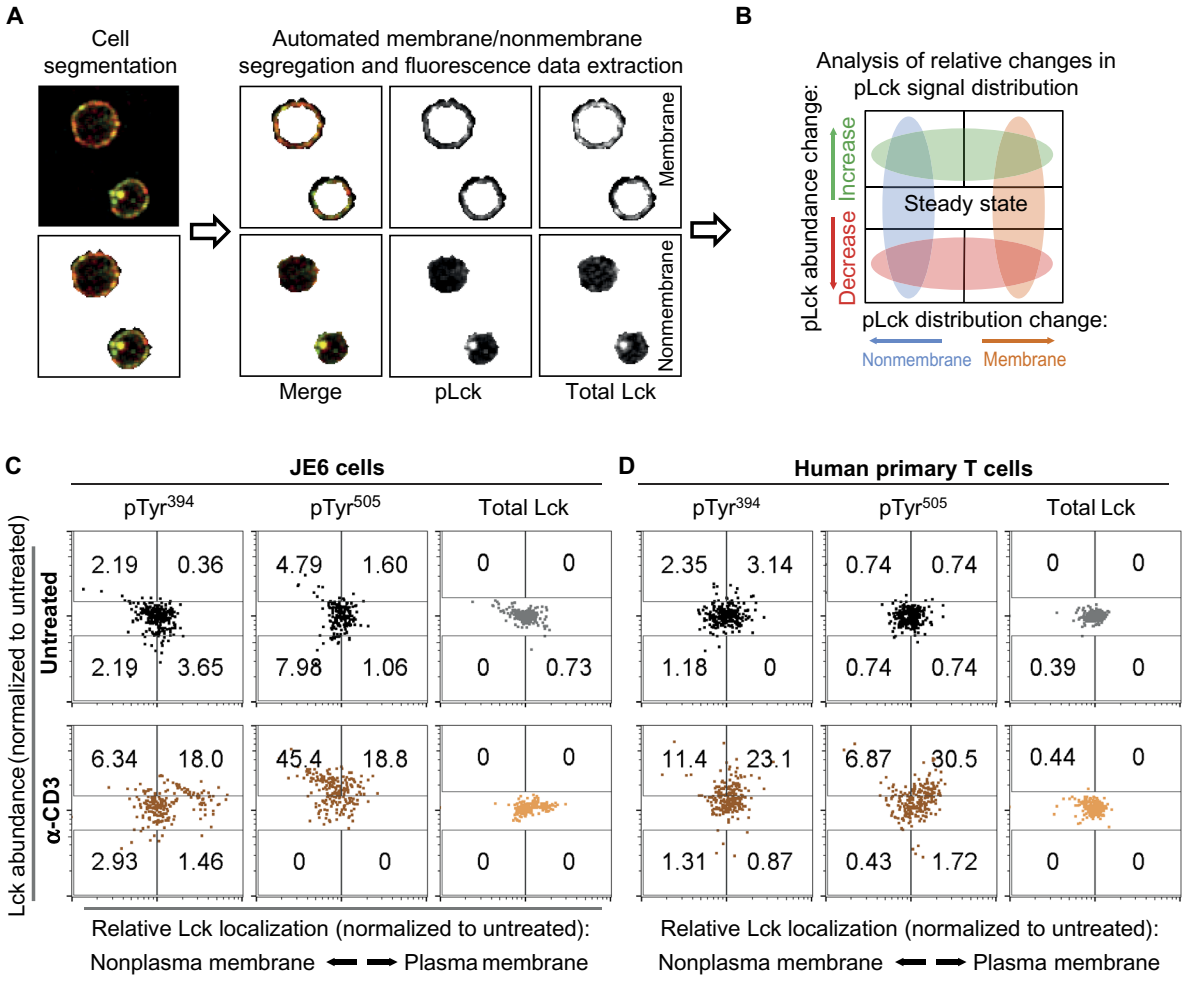

Fig. 7. TCR stimulation results in differential de novo phosphorylation of plasma membrane-localized versus non–plasma membrane-localized Lck. (**A**) Automated approach to segment cells into the membrane and nonmembrane (which include the intracellular Lck pool) compartments. Fluorescence signals for every cell compartment were then extracted and converted into a cytometry data set. (**B**) Schematic representation of possible changes in pLck abundance (*y* axis) and the relative subcellular distribution of pLck (*x* axis). (**C**) Subcellular analysis of Lck phosphorylation in the cells analyzed in Fig. 5. *Y* axis: Cellular abundance of Lck-pTyr^{394} (left), Lck-pTyr^{505} (middle), and total Lck (right) normalized to those of the untreated control cells. *X* axis: Relative subcellular distribution upon TCR stimulation of JE6 cells. Orange dot plots represent the stimulated cells normalized to the mean value of the respective untreated samples. The untreated cells (black and gray dot plots), whose values are distributed around the center of the plots because of normalization, are shown for comparison. Each dot represents one cell. Data are from more than 100 cells pooled from three independent experiments. (**D**) Experiments with human primary T cells were performed as described in (C). Data are from at least 100 cells pooled from three independent experiments.

The Tyr^{505}-mutated, open form of Lck is more enzymatically active than wild-type Lck in vitro (*14*, *15*). In contrast, we observed that cells expressing wild-type versus the Y505F mutant TqLck-V2 constructs exhibited comparable Ca^{2+} flux and ERK phosphorylation upon TCR stimulation. This observation could be explained either by the need for de novo Tyr^{394} phosphorylation or alternatively, according to the standby model, by recruitment of active Lck or unmasking of the ITAM phosphorylation sites. Our data on the Y394F/Y505F double mutant, however, underline a need for Tyr^{394} phosphorylation to induce TCR-proximal signaling. Consistent with this, we observed de novo phosphorylation of Tyr^{394} upon TCR stimulation at a single-cell level using an optimized SOP for immunofluorescence analysis of endogenous Lck. Furthermore, the optimized Lck staining procedure showed that the TCR-induced increase in Tyr^{394} phosphorylation preferentially occurred at the plasma membrane in both primary human T cells and JE6 cells (likely in close proximity to the TCR-CD3-ζ complex). This observation is consistent with our previous finding showing that conformational changes in Lck mainly occur at the contact site between the T cell and the antigen-loaded APC (*6*). However, we noted differences in the localization of de novo phosphorylated Tyr^{394} and Tyr^{505} when we directly compared JE6 cells with primary human T cells. Whereas in JE6 cells TCR-mediated phosphorylation of Tyr^{394} preferentially occurred at the plasma membrane, phosphorylation of Tyr^{505} was primarily observed in the non–plasma membrane compartment. In contrast, both residues were preferentially phosphorylated at the plasma membrane in primary human T cells. We envisage two hypotheses to explain this difference between the transformed JE6 cell line and the primary T cells. First, differential accessibility of the two tyrosines to their regulatory components (for example, CD45 or Csk) might provide a molecular explanation for this finding. Second, it is also possible that JE6 cells have alterations in intracellular protein trafficking that may, in turn, result in the differential distribution of Tyr^{505}-phosphorylated Lck

in the steady state and thus in different relative changes of protein distribution. Consistent with this, we found in PP2-treated cells reduced phosphorylation of both Tyr^{394} and Tyr^{505} in human T cells compared to that in JE6 cells. This is consistent with findings showing different fractions of prephosphorylated Lck in unstimulated Jurkat cells versus primary human T cells (*5*). Clearly, additional studies are required to assess this important issue.

In conclusion, using the optimized protocol for the staining of Lck in combination with FLIM/FRET measurements with the second-generation TqLck-V2 biosensor, we provide evidence that TCR-induced de novo phosphorylation of Tyr^{394} together with the conformational opening of Lck are crucial for Lck-mediated ITAM phosphorylation and the initiation of T cell activation. In addition, we describe an SOP for the staining of Lck in T cells that could be beneficial to all T cell biologists to obtain comparable and thus more interpretable data on the phosphorylation status and subcellular localization of Lck in T cells. Finally, if the anti-$pTyr^{394}$/$pTyr^{505}$ staining protocol is combined with antibodies that are capable of faithfully detecting other Src family kinases, our SOP may also be useful for scientists who are interested in the analysis of Src family kinases that are pivotal in many signaling processes in various other cell types.

MATERIALS AND METHODS

Cells and transfection

Approval for experiments involving human T cells was obtained from the ethics committee of the Medical Faculty at the Otto von Guericke University, Magdeburg, Germany, with permission number [107/09]. Informed consent was obtained in writing in accordance with the Declaration of Helsinki. Peripheral blood mononuclear cells collected from healthy volunteers were isolated by Ficoll gradient (Biochrom) centrifugation of heparinized blood at 512*g* for 30 min (without braking). The $CD4^+$ subpopulation was purified by negative selection T cell isolation kits (autoMACS, Miltenyi Biotec). Primary $CD4^+$ T cells, JE6 cells (*35*), and JCaM 1.6 (*3*) cells were cultured and transfected by established electroporation or retroviral transfection techniques (*36*), as described in the Supplementary Materials.

Expression vectors

pMBMN-Z vectors (Addgene, deposited by G. Nolan, Stanford University) containing the first-generation biosensor constructs encoding CLck-Y1, kinase-deficient Lck^{K273R}-YFP, and a CLckY2 variant with CFP inserted C-terminally of the SH3 domain have been described previously (*19*) and were provided by W. Paster and H. Stockinger (University of Vienna). The second-generation biosensor TqLck-V2 was generated from the CLckY2 variant by replacing the sequences encoding CFP and YFP with the sequences encoding mTurquoise2 (*20*) and mVenus (*21*), respectively, which were de novo–synthetized (Eurofins Genomics) for this purpose. A pRP expression vector for nontagged Lck under the control of a pEF1A promoter and parallel expression of GFP/Neo was obtained from VectorBuilder (www.vectorbuilder.com). All fusion protein genes were cloned into a pEF-BOS vector (*37*) for the transfection of JCaM 1.6 cells. V394F and Y505F point mutations were generated in the *tqLck-V2*–containing pEF-BOS vector by the QuikChange II XL Site-Directed Mutagenesis Kit (Agilent Technologies) using 5′-cggccacagagggccagttccagcctcagcct-3′ forward and 5′-aggctgaggctggaactggccctctgtggccg-3′ reverse primers for the Y505F mutation and 5′-gaggacaacgagttcacagccagggaggggc-3′ forward and 5′-gccccctccctggctgtgaactcgttgtcctc-3′ reverse primers for the Y394F mutation. To generate the Ala^{394} versions of the biosensor, two rounds of mutagenesis using first the 5′-cattgaggacaacgaggacacagccagggagggg-3′ forward and 5′-cccctccctggctgtggactcgttgtcctcaatg-3′ reverse primers and then the 5′-cattgaggacaacgaggccacagccagggagggg-3′ forward and 5′-cccctccctggctgtggcctcgttgtcctcaatg-3′ reverse primers were applied. All constructs were verified by sequencing.

TCR stimulation

To detect Lck phosphorylation by Western blotting or immunofluorescence, 5×10^6 JE6 cells or $CD4^+$ primary human T cells in RPMI 1640 medium were left untreated or treated with 10 μM PP2 (Merck Millipore) for 30 min at 37°C, 1 mM PV (Na_3VO_4 mixed with 1% H_2O_2) for 2 min at 37°C, or anti-CD3ε (10 μg/ml, clone UCHT1, eBioscience) for 2 min. The treatment was stopped by centrifuging the cells at 5900*g* for 30 s and washing with ice-cold phosphate-buffered saline (PBS). To measure ERK phosphorylation and Ca^{2+} flux, anti-human TCR IgM hybridoma supernatant (clone C305, provided by A. Weiss, University of California, San Francisco) was added in a ratio of 1:1 either for 3 min (for ERK phosphorylation measurement) or during fluorescence-activated cell sorting acquisition (for Ca^{2+} flux measurement). For FLIM measurement, JCaM 1.6 cells transfected with the biosensor variants were washed twice in 1 ml of Krebs-Ringer solution [10 mM Hepes (pH 7.0), 140 mM NaCl, 4 mM KCl, 1 mM $MgCl_2$, 10 mM glucose, and 1 mM $CaCl_2$] and plated on poly-L-lysine–coated glass-bottom dishes (MatTek). The cells were stimulated during acquisition with soluble anti-human CD3ε antibody (5 μg/ml, clone UCHT1, eBioscience).

Western blotting analysis

Cells were stimulated or left untreated as described in the figure legends, lysed in buffer containing 1% lauryl maltoside (*N*-dodecyl β-maltoside), 1% NP-40, 1 mM Na_3VO_4, 1 mM phenylmethylsulfonyl fluoride, 10 mM NaF, 10 mM EDTA, 50 mM tris (pH 7.5), and 150 mM NaCl for 20 min on ice. Lysates were incubated at 95°C for 7 min in sample buffer containing β-mercaptoethanol before loading onto 10% SDS–polyacrylamide gel electrophoresis gels. Proteins were then blotted onto nitrocellulose membranes. The membrane was blocked with tris-buffered saline (TBS) containing 5% milk powder at room temperature. Primary antibody pairs [mouse anti-Lck (clone 3A5, Santa Cruz Biotechnology) with either rabbit anti-pLck (Y505, Cell Signaling) or anti-pSrc (pY416, recognizing $pTyr^{394}$ of Lck; clone D49G4, Cell Signaling)] were incubated in TBS containing 5% bovine serum albumin (BSA). Goat anti-rabbit IRDye 680LT and goat anti-rabbit IRDye 800CW (both from LI-COR Biotechnology) or horseradish peroxidase–conjugated goat anti-rabbit (Dianova) were used as secondary antibodies. Signal intensities were determined by scanning the membranes with an Odyssey Infrared Imager (LI-COR Biotechnology) or with the ECL detection system (Amersham Pharmacia) and analyzed by the ImageJ gel analysis plug-in (http://imagej.nih.gov/ij/). The abundances of the proteins of interest were relative to that of the loading control β-actin (which was detected with mouse anti–β-actin; clone AC15, Sigma) and normalized to that of the untreated control cells.

Immunofluorescence acquisition and analysis

After treatment, the cells were transferred to adhesion slides (Marienfeld) and allowed to settle down for 10 min before fixation by 1% PFA and 0.02% GA in PBS for 15 min. Transfer and fixation were performed on ice. The cells were permeabilized for 10 min with 0.2% Triton X-100 (Sigma) in PBS and blocked with 1% BSA/0.1% Tween

20 (Sigma) in PBS. Rabbit anti-pSrc Y416 (which recognizes $pTyr^{394}$ of Lck), rabbit anti-Lck Tyr^{505} (both polyclonal, Cell Signaling), and mouse anti-Lck (clone 3A5, Santa Cruz Biotechnology) were used as primary antibodies. Alexa Fluor 555–labeled goat anti-rabbit IgG (Cell Signaling), Alexa Fluor 488–labeled goat anti-mouse IgG and goat anti-rabbit IgG (Cell Signaling), and Atto 550–labeled goat anti-mouse IgG2b (Antibodies-Online) were used as secondary antibodies. All incubations and washing steps were performed at room temperature in blocking buffer. Imaging was performed with a Leica TCS SP2 confocal laser scanning microscope (Leica) with a Leica IRE2 stand equipped with a 63× 1.40 HCX APO CS objective (Leica), an argon laser (488 nm), and a HeNe laser (543 nm). To avoid spectral overlap, the samples were sequentially scanned with a beam splitter HFT 488/543/633. Green and red fluorescence emission were read out at 500 to 551 nm and 571 to 626 nm, respectively. Image data were acquired, stored, and analyzed with a pixel depth of 8 bits. The cells were segmented into plasma membrane and non–plasma membrane compartments automatically with a threshold-based algorithm in the ImageJ software using the total Lck signal. Segmentation errors that occurred during the detection of Jurkat cells (for example, because of heterogenous membrane staining or cell-cell contacts) were corrected manually. The intracellular Lck pools were marked and segmented manually. From these data, the five segments analyzed, which included the plasma membrane, inner compartment without intracellular pool, intracellular pool, non–plasma membrane compartment (inner compartment plus intracellular pool), and total cell, were derived. For quantitative analysis, the data extracted from the segmented images were normalized to the mean value of the untreated controls of each respective experiment for each segment in a single cell–based manner. For total Lck, values from the double staining with $pTyr^{394}$ and $pTyr^{505}$ were pooled, and 50% of the values were used for the analysis to have equivalent numbers of events. Fluorescence ratios (plasma membrane to inner compartment without intracellular pool, intracellular pool to inner compartment without intracellular pool, and plasma membrane to nonmembrane compartment) were determined for each cell. The resulting tables of fluorescence ratios and total cell fluorescence values were converted into cytometry-compatible files (.fcs) with DISCit (*28*) and analyzed with FlowJo software (Tree Star).

Flow cytometric analysis

Transfected JCaM 1.6 cells were purified by Ficoll gradient to remove dead cells 16 hours after transfection. To measure ERK phosphorylation, cells were washed twice with PBS without Ca^{2+} and Mg^{2+} (Millipore) at room temperature, and ~1×10^6 cells were resuspended in RPMI medium (without BSA) and incubated for 5 min at 37°C, stimulated as described in the figure legends, and centrifuged at 3300*g* for 45 s. The cell pellets were immediately resuspended in ice-cold PFA, fixed at 37°C for 10 min, resuspended in cold 90% methanol, and incubated on ice for 30 min. The cells were then washed with 0.5% BSA in PBS and stained with a rabbit anti-human pERK primary antibody (Cell Signaling) and APC-conjugated anti-rabbit IgG (H+L) secondary antibody $F(ab')_2$ fragment (Dianova). Cells were analyzed with an LSRFortessa (BD Biosciences). To measure $pTyr^{394}$ and $pTyr^{505}$ by flow cytometry, the cells were permeabilized, blocked, and stained as described for fluorescence microscopy. For JE6 cells, all cells were analyzed, whereas for transiently transfected JCaM 1.6 cells, cells with physiological amounts of biosensor (see figs. S1 and S6 for details) were selected by gating on fluorescence-intermediate cells as shown in fig. S1 (A to C) (excitation, 488 nm; emission, 515 to 545 nm). The lower boundary of the pERK-positive gate was defined as the 98th percentile of nonstimulated, biosensor-negative cells in every experiment. To measure Ca^{2+} flux, ~2×10^6 cells were resuspended in indicator-free Gibco 1× RPMI 1640 medium supplemented with 10% fetal calf serum (FCS) and incubated with 5 μM Indo-1 AM (Invitrogen, Molecular Probes) at 37°C for 45 min. A 10-fold volume of indicator-free Gibco 1× RPMI 1640 medium with 10% FCS was then added, and the cells were incubated for 45 min at 37°C. Measurements were performed with an LSRI flow cytometer (BD Biosciences) equipped with a helium-cadmium laser (BD Biosciences) at 325 nm, and the 390- to 420-nm (high cytoplasmic Ca^{2+})–to–500- to 520-nm (low cytoplasmic Ca^{2+}) emission ratio was used to determine Ca^{2+} flux. Ionomycin (10 μg/ml, Sigma Aldrich) was added to the samples at the end of the measurement as a positive control to measure maximum Ca^{2+} flux. Ca^{2+} signal increase was determined from the mean 80th percentile over the period between 50 and 75 s after stimulation.

FLIM measurement and analysis

Cells were preselected for subsequent analysis by FLIM on the basis of having a rounded shape and low surface spreading when analyzed by transmitted light and for exhibiting intermediate fluorescence as well as both membrane and intracellular pool localization of the biosensor when analyzed by epifluorescence (see Fig. 4A and fig. S2, A and B). Time- and Space Correlated Single Photon Counting (TSCSPC) was used for wide-field, nonscanning FLIM as previously described (*29*, *32*, *38*); for a detailed setup description, see the Supplementary Materials. In brief, the cells were excited with an 8 MHz–pulsed frequency-doubled laser (Spectra-Physics) at 420 nm. An IX81 inverted microscope (Olympus) was used to collect the fluorescence signal through the objective reflected to the side port of the microscope after passing a 460-nm long-pass emission filter. A 505-nm beam splitter and 460- to 500-nm and 520- to 560-nm bandpass filters were used to detect donor and acceptor fluorescence, respectively. The instrument response function (IRF) was used in the analysis of time domain FLIM data. A reference dye (Auramine, Sigma-Aldrich, saturated solution in H_2O) with known short lifetime (86 ps) was used. The IRF measurements were performed with exactly the same wavelengths and optical elements (beam splitters and filters) in front of the FLIM detector as were used in the final measurements. A theoretical model decay was convolved with the measured IRF, and the result was compared with the recorded fluorescence decay, which resulted in a more precise, theoretical decay of the sample. The FLIM measurements were performed and analyzed as previously described (*6*, *32*, *38*). The fluorescence decays were analyzed by a Levenberg-Marquardt nonlinear least-squares algorithm with the MATLAB software package, version R12. The decays were modeled by the convolution product of a two-exponential theoretical model with the IRF:

$$I(t) = \mathrm{IRF}(t) \otimes \Sigma_i a_i \exp^{-t/T_i}$$

where a_i is the relative contribution of fluorescent species characterized by the fluorescence lifetime T_i. To visualize the spatial distribution of different excited states (high or low FRET signals) of the fluorophores inside a cell, the mean lifetimes were plotted as previously described (*39*). The resulting pseudocolor-coded lifetime maps show the distribution of mean lifetimes and thus of the distance of the

two fluorophores acting as donor and acceptor. For quantitative analysis, all photons collected were included in the determination of mean lifetimes. For data visualization by pseudocolor-coded lifetime maps, a rolling circle background subtraction (1-μm radius) and threshold adjustment were performed with the Fiji software (*40*). The pixels below the threshold were set to black.

Statistical analysis

Ca^{2+} and pERK flow cytometry experiments, Western blotting–based quantification of pLck abundance, steady-state FLIM lifetimes, and the extent of FLIM change upon TCR stimulation among different biosensor mutants were analyzed by one-way analysis of variance (ANOVA) with a Tukey posttest for multiple cross-comparisons. Fluorescence lifetime changes within individual cells upon TCR stimulation, and changes in the ratios between the total biosensor and either $pTyr^{394}$ or $pTyr^{505}$ were analyzed with Wilcoxon matched-pairs tests. The ratios of pLck to total Lck in the SOP were analyzed by two-way ANOVA with the individual experiments as a row variable and the experimental conditions as a column variable and, where more than two experimental conditions were applied, with a Bonferroni posttest. All analyses were performed with Prism software (version 6.04, GraphPad).

SUPPLEMENTARY MATERIALS

www.sciencesignaling.org/cgi/content/full/10/462/eaaf4736/DC1

Methods

Fig. S1. Efficiency of the reconstitution of TCR-proximal signaling in T cells by transient transfection with plasmids encoding fluorescently tagged Lck variants.

Fig. S2. Comparison of the conformational dynamics of the Y394A and Y394F single mutant and the Y394A/Y505F and Y394F/Y505F double mutant Lck biosensors.

Fig. S3. Influence of mutating Tyr^{394} or Tyr^{505} on the abundance of TqLck-V2 in transiently transfected JCaM 1.6 cells.

Fig. S4. Capability of the wild-type and tyrosine-mutated TqLck-V2 biosensors to reconstitute TCR-proximal signaling.

Fig. S5. An optimized staining protocol for investigating Lck at the single-cell level.

Fig. S6. Influence of T cell activation by mouse anti-CD3 IgG1 on the detection of Lck with a primary mouse IgG2b antibody against total Lck.

Fig. S7. Analysis of Tyr^{505} phosphorylation upon TCR stimulation of JCaM 1.6 cells expressing constitutively closed TqLck-V2 biosensors.

Table S1. Comparison of the ECFP and Turquoise2 FRET donors and of the ECFP-EYFP and Tq-V2 FRET pairs.

REFERENCES AND NOTES

1. T. J. Molina, K. Kishihara, D. P. Siderovski, W. van Ewijk, A. Narendran, E. Timms, A. Wakeham, C. J. Paige, K.-U. Hartmann, A. Veillette, D. Davidson, T. W. Mak, Profound block in thymocyte development in mice lacking $p56^{lck}$. *Nature* **357**, 161–164 (1992).
2. B. Seddon, G. Legname, P. Tomlinson, R. Zamoyska, Long-term survival but impaired homeostatic proliferation of naïve T cells in the absence of $p56^{lck}$. *Science* **290**, 127–131 (2000).
3. M. A. Goldsmith, A. Weiss, Isolation and characterization of a T-lymphocyte somatic mutant with altered signal transduction by the antigen receptor. *Proc. Natl. Acad. Sci. U.S.A.* **84**, 6879–6883 (1987).
4. J. E. Smith-Garvin, G. A. Koretzky, M. S. Jordan, T cell activation. *Annu. Rev. Immunol.* **27**, 591–619 (2009).
5. K. Nika, C. Soldani, M. Salek, W. Paster, A. Gray, R. Etzensperger, L. Fugger, P. Polzella, V. Cerundolo, O. Dushek, T. Höfer, A. Viola, O. Acuto, Constitutively active Lck kinase in T cells drives antigen receptor signal transduction. *Immunity* **32**, 766–777 (2010).
6. A. Stirnweiss, R. Hartig, S. Gieseler, J. A. Lindquist, P. Reichardt, L. Philipsen, L. Simeoni, M. Poltorak, C. Merten, W. Zuschratter, Y. Prokazov, W. Paster, H. Stockinger, T. Harder, M. Gunzer, B. Schraven, T cell activation results in conformational changes in the Src family kinase Lck to induce its activation. *Sci. Signal.* **6**, ra13 (2013).
7. O. Ballek, J. Valečka, J. Manning, D. Filipp, The pool of preactivated Lck in the initiation of T-cell signaling: A critical re-evaluation of the Lck standby model. *Immunol. Cell Biol.* **93**, 384–395 (2015).
8. A. L. Burkhardt, B. Stealey, R. B. Rowley, S. Mahajan, M. Prendergast, J. Fargnoli, J. B. Bolen, Temporal regulation of non-transmembrane protein tyrosine kinase enzyme activity following T cell antigen receptor engagement. *J. Biol. Chem.* **269**, 23642–23647 (1994).
9. E. H. Palacios, A. Weiss, Function of the Src-family kinases, Lck and Fyn, in T-cell development and activation. *Oncogene* **23**, 7990–8000 (2004).
10. M. Bergman, T. Mustelin, C. Oetken, J. Partanen, N. A. Flint, K. E. Amrein, M. Autero, P. Burn, K. Alitalo, The human p50csk tyrosine kinase phosphorylates p56lck at Tyr-505 and down regulates its catalytic activity. *EMBO J.* **11**, 2919–2924 (1992).
11. W. Xu, A. Doshi, M. Lei, M. J. Eck, S. C. Harrison, Crystal structures of c-Src reveal features of its autoinhibitory mechanism. *Mol. Cell* **3**, 629–638 (1999).
12. W. Xu, S. C. Harrison, M. J. Eck, Three-dimensional structure of the tyrosine kinase c-Src. *Nature* **385**, 595–602 (1997).
13. H. L. Ostergaard, D. A. Shackelford, T. R. Hurley, P. Johnson, R. Hyman, B. M. Sefton, I. S. Trowbridge, Expression of CD45 alters phosphorylation of the lck-encoded tyrosine protein kinase in murine lymphoma T-cell lines. *Proc. Natl. Acad. Sci. U.S.A.* **86**, 8959–8963 (1989).
14. E. Hui, R. D. Vale, In vitro membrane reconstitution of the T-cell receptor proximal signaling network. *Nat. Struct. Mol. Biol.* **21**, 133–142 (2014).
15. U. D'Oro, K. Sakaguchi, E. Appella, J. D. Ashwell, Mutational analysis of Lck in CD45-negative T cells: Dominant role of tyrosine 394 phosphorylation in kinase activity. *Mol. Cell. Biol.* **16**, 4996–5003 (1996).
16. J. S. Hardwick, B. M. Sefton, Activation of the Lck tyrosine protein kinase by hydrogen peroxide requires the phosphorylation of Tyr-394. *Proc. Natl. Acad. Sci. U.S.A.* **92**, 4527–4531 (1995).
17. H. Xu, D. R. Littman, The kinase-dependent function of Lck in T-cell activation requires an intact site for tyrosine autophosphorylation. *Ann. N. Y. Acad. Sci.* **766**, 99–116 (1995).
18. A. Alonso, N. Bottini, S. Bruckner, S. Rahmouni, S. Williams, S. P. Schoenberger, T. Mustelin, Lck dephosphorylation at Tyr-394 and inhibition of T cell antigen receptor signaling by *Yersinia* phosphatase YopH. *J. Biol. Chem.* **279**, 4922–4928 (2004).
19. W. Paster, C. Paar, P. Eckerstorfer, A. Jakober, K. Drbal, G. J. Schütz, A. Sonnleitner, H. Stockinger, Genetically encoded Förster resonance energy transfer sensors for the conformation of the Src family kinase Lck. *J. Immunol.* **182**, 2160–2167 (2009).
20. J. Goedhart, D. von Stetten, M. Noirclerc-Savoye, M. Lelimousin, L. Joosen, M. A. Hink, L. van Weeren, T. W. J. Gadella Jr., A. Royant, Structure-guided evolution of cyan fluorescent proteins towards a quantum yield of 93%. *Nat. Commun.* **3**, 751 (2012).
21. G.-J. Kremers, J. Goedhart, E. B. van Munster, T. W. J. Gadella Jr., Cyan and yellow super fluorescent proteins with improved brightness, protein folding, and FRET Förster radius. *Biochemistry* **45**, 6570–6580 (2006).
22. S. C. Ley, M. Marsh, C. R. Bebbington, K. Proudfoot, P. Jordan, Distinct intracellular localization of Lck and Fyn protein tyrosine kinases in human T lymphocytes. *J. Cell Biol.* **125**, 639–649 (1994).
23. O. Anton, A. Batista, J. Millán, L. Andrés-Delgado, R. Puertollano, I. Correas, M. A. Alonso, An essential role for the MAL protein in targeting Lck to the plasma membrane of human T lymphocytes. *J. Exp. Med.* **205**, 3201–3213 (2008).
24. J. H. Hanke, J. P. Gardner, R. L. Dow, P. S. Changelian, W. H. Brissette, E. J. Weringer, B. A. Pollok, P. A. Connelly, Discovery of a novel, potent, and Src family-selective tyrosine kinase inhibitor. Study of Lck- and FynT-dependent T cell activation. *J. Biol. Chem.* **271**, 695–701 (1996).
25. V. Imbert, J. F. Peyron, D. Farahi Far, B. Mari, P. Auberger, B. Rossi, Induction of tyrosine phosphorylation and T-cell activation by vanadate peroxide, an inhibitor of protein tyrosine phosphatases. *Biochem. J.* **297** (Pt. 1), 163–173 (1994).
26. A. M. Nyakeriga, H. Garg, A. Joshi, TCR-induced T cell activation leads to simultaneous phosphorylation at Y505 and Y394 of $p56^{lck}$ residues. *Cytometry* **81A**, 797–805 (2012).
27. S. Dornan, Z. Sebestyen, J. Gamble, P. Nagy, A. Bodnar, L. Alldridge, S. Doe, N. Holmes, L. K. Goff, P. Beverley, J. Szollosi, D. R. Alexander, Differential association of CD45 isoforms with CD4 and CD8 regulates the actions of specific pools of $p56^{lck}$ tyrosine kinase in T cell antigen receptor signal transduction. *J. Biol. Chem.* **277**, 1912–1918 (2002).
28. H. D. Moreau, F. Lemaître, E. Terriac, G. Azar, M. Piel, A.-M. Lennon-Dumenil, P. Bousso, Dynamic in situ cytometry uncovers T cell receptor signaling during immunological synapses and kinapses in vivo. *Immunity* **37**, 351–363 (2012).
29. M. Jose, D. K. Nair, C. Reissner, R. Hartig, W. Zuschratter, Photophysics of Clomeleon by FLIM: Discriminating excited state reactions along neuronal development. *Biophys. J.* **92**, 2237–2254 (2007).
30. S. P. Laptenok, J. W. Borst, K. M. Mullen, I. H. M. van Stokkum, A. J. W. G. Visser, H. van Amerongen, Global analysis of Förster resonance energy transfer in live cells measured by fluorescence lifetime imaging microscopy exploiting the rise time of acceptor fluorescence. *Phys. Chem. Chem. Phys.* **12**, 7593–7602 (2010).

31. M. Millington, G. J. Grindlay, K. Altenbach, R. K. Neely, W. Kolch, M. Benčina, N. D. Read, A. C. Jones, D. T. F. Dryden, S. W. Magennis, High-precision FLIM-FRET in fixed and living cells reveals heterogeneity in a simple CFP–YFP fusion protein. *Biophys. Chem.* **127**, 155–164 (2007).
32. D. K. Nair, M. Jose, T. Kuner, W. Zuschratter, R. Hartig, FRET-FLIM at nanometer spectral resolution from living cells. *Opt. Express* **14**, 12217–12229 (2006).
33. A. J. W. G. Visser, S. P. Laptenok, N. V. Visser, A. van Hoek, D. J. S. Birch, J.-C. Brochon, J. W. Borst, Time-resolved FRET fluorescence spectroscopy of visible fluorescent protein pairs. *Eur. Biophys. J.* **39**, 241–253 (2010).
34. J. Rossy, D. M. Owen, D. J. Williamson, Z. Yang, K. Gaus, Conformational states of the kinase Lck regulate clustering in early T cell signaling. *Nat. Immunol.* **14**, 82–89 (2013).
35. A. Weiss, J. Imboden, D. Shoback, J. Stobo, Role of T3 surface molecules in human T-cell activation: T3-dependent activation results in an increase in cytoplasmic free calcium. *Proc. Natl. Acad. Sci. U.S.A.* **81**, 4169–4173 (1984).
36. S. Swift, J. Lorens, P. Achacoso, G. P. Nolan, Rapid production of retroviruses for efficient gene delivery to mammalian cells using 293T cell-based systems. *Curr. Protoc. Immunol.* **Chapter 10**, Unit 10.17C (2001).
37. S. Mizushima, S. Nagata, pEF-BOS, a powerful mammalian expression vector. *Nucleic Acids Res.* **18**, 5322 (1990).
38. R. Hartig, Y. Prokazov, E. Turbin, W. Zuschratter, Wide-field fluorescence lifetime imaging with multi-anode detectors. *Methods Mol. Biol.* **1076**, 457–480 (2014).
39. M. Vitali, F. Picazo, Y. Prokazov, A. Duci, E. Turbin, C. Götze, J. Llopis, R. Hartig, A. J. W. G. Visser, W. Zuschratter, Wide-Field Multi-Parameter FLIM: Long-term minimal invasive observation of proteins in living cells. *PLOS ONE* **6**, e15820 (2011).
40. J. Schindelin, I. Arganda-Carreras, E. Frise, V. Kaynig, M. Longair, T. Pietzsch, S. Preibisch, C. Rueden, S. Saalfeld, B. Schmid, J.-Y. Tinevez, D. J. White, V. Hartenstein, K. Eliceiri, P. Tomancak, A. Cardona, Fiji: An open-source platform for biological-image analysis. *Nat. Methods* **9**, 676–682 (2012).
41. M. A. Young, S. Gonfloni, G. Superti-Furga, B. Roux, J. Kuriyan, Dynamic coupling between the SH2 and SH3 domains of c-Src and Hck underlies their inactivation by C-terminal tyrosine phosphorylation. *Cell* **105**, 115–126 (2001).
42. J. A. Moroco, J. K. Craigo, R. E. Iacob, T. E. Wales, J. R. Engen, T. E. Smithgall, Differential sensitivity of Src-family kinases to activation by SH3 domain displacement. *PLOS ONE* **9**, e105629 (2014).

Acknowledgments: The excellent technical support of K. Baumgart, P. Gintschel, C. Merten, I. Meinert, and G. Höbbel is gratefully acknowledged. We thank W. Paster and H. Stockinger for providing the first-generation biosensor and A. Weiss for providing the C305 antibody. Funding: This work was supported by the Deutsche Forschungsgemeinschaft (SFB854-B19/02 to B.S. and L.S., SFB854-Z01/02 to A.J.M. and W.Z., MU 3744/2-1 to A.J.M., and BMBF 13N12675 to W.Z.). **Author contributions:** B.S., L.S., and A.J.M. conceived and designed the experiments; L.P., A.V.R., R.H., J.G., M.K., A.K., and M.P.P. performed the experiments; L.P., A.V.R., R.H., and A.J.M. evaluated the data; Y.P., E.T., A.W., and W.Z. provided critical technology; and B.S., L.S., and A.J.M. prepared the manuscript. **Competing interests:** The authors declare that they have no competing interests. **Data and materials availability:** Use of the plasmids encoding fluorescently tagged proteins requires a material transfer agreement.

Submitted 13 February 2016
Accepted 30 December 2016
Published 17 January 2017
10.1126/scisignal.aaf4736

Citation: L. Philipsen, A. V. Reddycherla, R. Hartig, J. Gumz, M. Kästle, A. Kritikos, M. P. Poltorak, Y. Prokazov, E. Turbin, A. Weber, W. Zuschratter, B. Schraven, L. Simeoni, A. J. Müller, De novo phosphorylation and conformational opening of the tyrosine kinase Lck act in concert to initiate T cell receptor signaling. *Sci. Signal.* **10**, eaaf4736 (2017).

De novo phosphorylation and conformational opening of the tyrosine kinase Lck act in concert to initiate T cell receptor signaling

Lars Philipsen, Amarendra V. Reddycherla, Roland Hartig, Janine Gumz, Matthias Kästle, Andreas Kritikos, Mateusz P. Poltorak, Yury Prokazov, Evgeny Turbin, André Weber, Werner Zuschratter, Burkhart Schraven, Luca Simeoni and Andreas J. Müller (January 17, 2017)

Science Signaling **10** (462), . [doi: 10.1126/scisignal.aaf4736]